# INTERACTION AT SEPARATION JOINTS OF THE I10/215 BRIDGE DURING EARTHQUAKES

P. K. Malhotra, M. J. Huang and A. F. Shakal

California Strong Motion Instrumentation Program
Division of Mines and Geology, California Department of Conservation

## ABSTRACT

A multi-span, curved, concrete box-girder bridge has been extensively instrumented by the California Strong Motion Instrumentation Program (CSMIP) in cooperation with the California Department of Transportation (Caltrans). On June 28, 1992, the bridge was shaken by the magnitude 7.5 Landers and magnitude 6.6 Big Bear earthquakes in Southern California. The epicenters of these earthquakes were 50 and 29 miles (81 and 46 km) from the bridge, respectively. All thirty-four strong-motion sensors installed on the bridge recorded its response to these earthquakes and provided an insightful set of response data. A striking aspect of the response is the presence of intermittent sharp spikes in nearly all of the acceleration records from sensors on the deck of the bridge. Among these the highest spike was $0.80g$ for the Landers and $1.00g$ for the Big Bear earthquake. The peak ground acceleration at the bridge site was only about $0.10g$ for both these earthquakes. With the aid of visual examination and simple analysis it is deduced that: (i) the spikes were caused by forces generated at separation joints between adjacent bridge segments by impacts and stretching of the cable restrainers; and (ii) the forces of impacts and cable stretching are directly proportional to the size of the spikes and can be estimated by the use of a simple formula.

## INTRODUCTION

The California Strong Motion Instrumentation Program (CSMIP) of the Division of Mines and Geology in the Department of Conservation is installing strong-motion sensors on different structures and ground sites in California. The bridge structure examined here is one of the more than 100 stations from which strong-motion records were obtained during the June 28, 1992 Landers and Big Bear earthquakes in California.

### Bridge Structure

The instrumented bridge (shown in Figure 1) is a multi-span, concrete structure that connects highways I-10 and I-215 in Southern California, approximately 53 miles (85 km) from downtown Los Angeles. The bridge is curved in plan with radii of 1,200 and 1,300 ft (365 and 396 m), and has a total length of 2,540 ft (774 m). The superstructure consists of a 41 ft (12.5 m) wide, 4-cell concrete box-girder that carries two lanes of traffic from eastbound I-10 to northbound I-215. There are five separation joints (hinges) in the box-girder that divide the bridge into six structures of different lengths and number of spans. The hinges are numbered 3, 7, 9, 11 and 13 in Figure 1. The box-girder is supported on single-column concrete bents and abutments that are monolithic with it. The columns are octagonal in shape and $8 \times 5.5$ ft ($2.4 \times 1.7$ m) in size. Their height ranges from 24 to 76 ft (7.3 to 23.2 m).

The bridge was designed by the California Department of Transportation (Caltrans) in 1969 and the construction was completed in 1973. During 1991-92 the bridge was retrofitted by Caltrans under a program to seismically upgrade bridges with single-column bents. One of the tasks of this retrofitting effort was to improve the connection at the hinges by tying the adjacent segments of the box-girder with new cable restrainers. A typical cable restrainer unit, shown in Figure 2, consists of twenty 0.75 in (1.9 cm) diameter cables, between 16 and 21 ft (4.9 and 6.4 m) long.

### Strong-Motion Instrumentation and Earthquake Records

Seismic instrumentation of the bridge by CSMIP was completed in early 1992. A total of thirty-four strong-motion sensors (accelerometers) were installed to measure the motions of selected points at the base of concrete columns, the abutments, and the bridge deck. Of particular interest in this instrumentation was the response at the hinges. Sensors were installed at each of the five hinges to measure the transverse motions of the adjacent bridge segments. At some hinges the longitudinal and vertical motions are also measured. Only selected sensors are shown by numbered arrows in Figure 1, where the arrows indicate the positive direction of motion measured by the sensors. Sensor 6, for example, measures the transverse motion at the base of Bent 3, and Sensor 10 measures the longitudinal motion of the left segment at Hinge 3. The positive motion measured by Sensors 6, 7 and 8 is in the radially inward direction. The positive motion measured by Sensor 10 is tangential to the bridge in the clockwise direction. The complete instrumentation scheme is discussed in detail by Huang and Shakal (1994).

The acceleration records for the Landers and Big Bear earthquakes from all thirty-four sensors on the bridge were included in three CSMIP data reports (Shakal et al., 1992; Huang et al., 1992; Darragh et al., 1993). The records obtained from sensors near the hinges were of special significance because of intermittent sharp spikes, as high as $1.00g$. The peak ground accelerations, however, were only about $0.10g$.

### Scope and Objectives

The objectives of this paper are: (i) to identify the mechanism(s) responsible for the observed spikes, and (ii) to estimate the magnitude of the forces involved. For this purpose records obtained during the Landers earthquake, only from Sensors 6, 7, 8 and 10, are studied here. These records are shown in Figure 3.

## SEISMIC INTERACTION AT A HINGE

A vertical section through Hinge 3 in Figure 2 shows that the right segment is supported by the left segment and rests on an elastomeric bearing pad. There is a horizontal separation between the two segments, provided to accommodate temperature-induced expansion; the separation gap had a width of 2 in (5 cm) at the time of construction. The actual width of the gap at the time of the earthquakes might have been different depending upon the effect of aging on concrete and temperature at the time of earthquakes. According to Caltrans design drawings, the cable restrainers were given an initial slack of approximately 2 in (5 cm) to allow free movement of the bridge segments during temperature variations.

At Hinge 3 the transverse motions of the left and the right segments of the box-girder are measured by Sensors 7 and 8, respectively. In addition, the longitudinal motion of the left segment is measured by Sensor 10. The acceleration records of these sensors, shown in Figure 3, contain a series of sharp spikes. These spikes are more clearly visible in the smaller, 9 second, segments of these records that are shown in Figure 4. Note that:

- The spikes appear in sets, occurring simultaneously in each of the three records in Figure 4; seven sets of spikes appeared during the 18.5 to 27.5 second interval.
- With the exception of Spike 3, the transverse spikes (in the records of Sensors 7 and 8) are equal in magnitude and opposite in direction to each other; the 3rd spike in these two records points in the same direction.

Spikes of similar nature can be observed in the published data from all hinges of the bridge during both Landers and Big Bear earthquakes (Shakal et al., 1992; Huang et al., 1992; Darragh et al., 1993).

Due to the absence of spikes in the base input motion, measured by Sensor 6 (see Figure 3), it is apparent that the observed spikes are not directly caused by the ground input motion. Whereas, the response without the spikes is a direct result of the amplification of ground motion through the height of the bridge, the spikes are caused by interaction between the adjacent bridge segments at the hinges. Three different mechanisms that might be responsible for the observed spikes are discussed below.

### Interaction Mechanisms

The equal and opposite transverse spikes (1, 2, 4, 5, 6 and 7 in Figure 4) are the result of a pair of self-balancing transverse forces generated at Hinge 3. Two mechanisms (Mechanisms 1 and 2) that may give rise to these forces are as follows:

Mechanism 1–Frictional Contact. In this mechanism, illustrated in Figure 5(a), the two adjacent segments of the box-girder, undergoing predominantly transverse motion, come in contact with each other. Upon contact a pair of equal and opposite frictional forces, $F_T$, are generated in the transverse direction. These forces are in turn responsible for the observed equal and opposite spikes in the transverse direction. Note that an axial compressive force, $F_L$, is also generated in this mechanism. This force is responsible for the longitudinal spike.

Mechanism 2–Cable Restraint. In this mechanism, illustrated in Figure 5(b), the two adjacent segments, undergoing predominantly transverse motion, move far enough away from one another that the cable restrainers between them become engaged and pull the two segments back toward each other. In this case the component of the cable forces in the transverse direction, $F_T$, is responsible for the spikes in that direction. The axial tensile force, $F_L$, equal in magnitude to the longitudinal component of the cable force, is responsible for the longitudinal spike in this mechanism.

After analyzing the longitudinal spikes in the next section it is deduced that the Spikes 1, 2, 5 and 6 were caused by Mechanism 1, and Spikes 4 and 7 were caused by Mechanism 2.

The 3rd set of spikes in Figure 4 can not be explained by either Mechanism 1 or 2 because the transverse spikes in this set are not equal and opposite to each other. A clue to the mechanism that might have given rise to the 3rd set of spikes is provided by the large longitudinal response corresponding to this set of spikes (see $A_{10}(t)$ in Figure 4). This mechanism is as follows:

**Mechanism 3–Head-on Impact**. Spikes in this mechanism are generated by a head-on impact between adjacent bridge segments undergoing predominantly longitudinal motion. The response in this case is, therefore, predominantly longitudinal, although a certain amount of transverse response is also generated. One possible cause of the transverse response is illustrated is Figure 6 in which two adjacent segments are shown to impact against each other at a slight angle. Upon impact a pair of transverse forces, $F_T$, pointing in the same transverse direction is generated which is responsible for nearly identical transverse spikes.

## FORCES OF INTERACTION

As already noted, each spike in the transverse direction is accompanied by a spike in the longitudinal direction, which should, more appropriately, be called a doublet because of its shape. Upon closer examination of the longitudinal response, $A_{10}(t)$ in Figure 4, it is seen that for Doublets 1, 2, 3, 5 and 6 a positive peak is followed by a negative peak, while for Doublets 4 and 7 it is vice-versa–a negative peak followed by a positive peak. The sign reversal of the doublet peaks is more clearly visible in Figure 7 where the lower two plots of Figure 4 are redrawn to a larger horizontal scale in the vicinity of Doublets 2 and 7. The shape of Doublet 2 in the record of Sensor 10 may be approximated by a single cycle of sinusoidal function, i.e.

$$A(t) = A_{max} \sin\left(\frac{2\pi t}{\tau}\right) \tag{1}$$

where $\tau$=the duration of the doublet and $A_{max}$=its amplitude. As previously mentioned, Doublet 2 was caused by an axial force generated by Mechanism 1 or 2. Whether the axial force is compressive or tensile will determine if the doublet was caused by Mechanism 1 or by Mechanism 2.

A simple model is used to determine the shape and size of the axial force pulse that produced Doublet 2, given by equation (1). In this model, shown in Figure 8(a), the segment of the box-girder to the left of Hinge 3 is represented by a semi-infinite rod of uniform cross-section area $\bar{A}$. An unknown axial force $F(t)$ is suddenly applied at the right end of this rod which produces an acceleration response at that end of the rod of the form given by equation (1) and shown in Figure 8(b). The objective is to determine the force $F(t)$ from this acceleration response. With the help of an analysis that made use of the one-dimensional wave propagation theory it is shown by Malhotra et al. (1994) that the axial force $F(t)$ has the following form:

$$F(t) = A_{max} \frac{c\rho\tau}{\pi} \left[\frac{1}{2}\left(1 - \cos\frac{2\pi t}{\tau}\right)\right] \times \bar{A} \tag{2}$$

in which $c$=the compression wave velocity is given by the following expression (Clough and Penzien 1993):

$$c = \sqrt{\frac{E}{\rho}} \tag{3}$$

where $E$=the Young's modulus of elasticity, and $\rho = w/g$=its mass density, obtained by dividing the weight density $w$ by the acceleration due to gravity $g$. The force $F(t)$ is plotted in Figure 8(c), below the assumed acceleration form shown in Figure 8(b). During time $\tau$ the force builds up from zero to a maximum value and then drops to zero again. Its positive sign implies that the force is compressive. Since the assumed acceleration form (Figure 8(b)) was chosen to approximate the shape of Doublet 2 in Figure 4, the doublet was, therefore, produced by a compressive force generated by impacts between the adjacent segments in Mechanism 1.

The results of the above analysis are summarized in the top row of Table I which essentially states that Mechanism 1 produces equal and opposite spikes in the transverse direction and a sinusoidal doublet in the longitudinal direction. Spikes 1, 2, 5 and 6 in Figure 4 were, therefore, caused by Mechanism 1. Rows two and three of Table I are generated by simple deduction. It is stated in the second row that Mechanism 2, similar to Mechanism 1, produces equal and opposite spikes in the transverse direction but a reverse sinusoidal doublet in the longitudinal direction (caused by an axial tensile force). Spikes 4 and 7 were, therefore, caused by Mechanism 2. In the third row of Table I, Mechanism 3 is shown to produce transverse spikes that are nearly equal to each other, and a longitudinal doublet that has a sinusoidal shape similar to Mechanism 1. Spike 3 was, therefore, caused by Mechanism 3.

**Forces of Impact**

Substituting the term in the square brackets in equation (2) by its maximum value of unity, the expression for the maximum value of the force $F_{max}$ is obtained as follows:

$$F_{max} = A_{max}\frac{c\tau\rho}{\pi} \times \bar{A} \tag{4}$$

By making use of equation (4) one can compute the forces generated at Hinge 3 from the size (amplitude and duration) of the longitudinal doublets. For Doublet 2 (Figure 6), $A_{max}=0.24g$, and $\tau=0.04$ sec. The compression wave velocity $c$, obtained from equation (3) by using Young's modulus of elasticity $E$=3,400 ksi (23.4 GPa) and weight density $w=\rho g$=145 lb/ft$^3$ (22.8 kN/m$^3$) is 10,400 ft/sec (3,200 m/sec). The cross-section area of the box-girder, estimated from construction drawings is $\bar{A}$=10,000 in$^2$ (6.45 m$^2$). Upon substituting the values of various quantities in (4) one obtains, $F_{max}$=320 kips (1,450 kN). Assuming that the entire cross-section of the box-girder comes in contact when the two segments collide, the maximum compressive stress $\sigma_{max}=F_{max}/\bar{A}$=32 psi (220 kPa).

The largest doublet in the record of Sensor 10 is Doublet 3 (see Figure 4). Its large size is not unexpected because it is associated with Mechanism 3 in which a head-on impact occurs between the adjacent bridge segments. Although the shape of Doublet 3 is not strictly sinusoidal a rough estimate of the force responsible for this doublet can still be obtained by

the use of the simple formula given by (4). This force is nearly ten times (≈3,000 kips) the force that caused Doublet 2, and the corresponding stress $\sigma_{max}$=300 psi.

### Tensile Forces in Cable Restrainers

As previously noted, Doublets 7 in Figure 7 was caused by Mechanism 2 by sudden engagement of the cable restrainers between the adjacent segments. Equation (4) can also be used to estimate the cable forces from the size of Doublet 7, for which $A_{max}$=−0.10$g$ and $\tau$=0.10 sec. Upon substituting these into (4), one obtains the net maximum tensile force in the box-girder and hence in the cable restrainers to be 330 kips (1,470 kN). This gives an average tensile force in each of the twenty cables to be 16.5 kips (73.5 kN). The actual force in a cable may be significantly larger since not all the cables are necessarily engaged at the same time. The stress in a 0.75 in diameter cable corresponding to a tensile force of 16.5 kips is 37.4 ksi (257 MPa).

### Actual vs. Allowable Stresses

In accordance with Caltrans "Bridge Design Specifications" (1990) the allowable compressive stress for concrete is 2 ksi (13.8 MPa), and the cracking stress is 530 psi (3.65 MPa). The maximum value of the compressive stress pulse generated by impacts in Mechanism 3 was estimated to be approximately 300 psi (2.07 MPa). This value is only 15% of the allowable value. A compressive pulse is, however, reflected as a tensile pulse, of equal magnitude, from the free end of the medium in which it travels (Clough and Penzien 1993). In other words, a compressive pulse generated at Hinge 3 is reflected as a tensile pulse from Hinge 7. A tensile stress of 300 psi is quite considerable for concrete, but still only 57% of the cracking stress.

As noted above the maximum stress induced in the cable restrainers was estimated to be 37.4 ksi (257 MPa). This value is 21% of the yield stress $F_y$=176 ksi (1,220 GPa) given by the Caltrans "Bridge Design Aids" (1991).

## CONCLUSIONS

This paper was focused on the interpretation and analysis of sharp spikes in the acceleration records obtained during a recent California earthquake from an instrumented concrete bridge. The principal conclusions are as follows:

1. The spikes were caused by forces generated at the separation joints (hinges) by the interaction of adjacent segments of the box-girder. The interaction between adjacent segments occurred both by impacts and by engagement of the cable restrainers that tie them together.

2. The forces of impact and cable restraining can be estimated from the amplitude and duration of the acceleration spikes using a simple formula. Results obtained from the strong-motion records indicate that reasonably high forces were generated at the hinges during the 1992 Landers earthquake. However, the resulting stresses estimated were below the yield values for the cable restrainers and concrete.

## REFERENCES

"Bridge Design Aids (14-16)," (1991) California Department of Transportation.

"Bridge Design Specifications (9-7)," (1990) California Department of Transportation.

Clough, R. W., and Penzien, J. (1993) "Dynamics of Structures," McGraw-Hill, Inc., 2nd Edition.

Darragh, R., Cao, T., Huang, M., Shakal, A. (1993) "Processed CSMIP Strong-Motion Records From the Landers and Big Bear, California Earthquakes of 28 June 1992: San Bernardino–I10/215 Interchange," California Department of Conservation, Division of Mines and Geology, Office of Strong Motion Studies, Report OSMS 93-08.

Huang, M., Shakal, A., Cao, T., Sherburne, R., Sydnor, R., Fung, P., Malhotra, P., Cramer, C., Su, F., Darragh, R., and Wampole, J. (1992) "CSMIP Strong Motion Records From the Big Bear, California Earthquake of 28 June 1992," California Department of Conservation, Division of Mines and Geology, Office of Strong Motion Studies, Report OSMS 92-10.

Huang, M., and Shakal, A. (1994) "CSMIP Strong-Motion Instrumentation and Records from the I10/215 Interchange Bridge near San Bernardino," *Earthquake Spectra*, submitted for publication.

Shakal, A., Huang, M., Cao, T., Sherburne, R., Sydnor, R., Fung, P., Malhotra, P., Cramer, C., Su, F., Darragh, R., and Wampole, J. (1992) "CSMIP Strong Motion Records From the Landers, California Earthquake of 28 June 1992," California Department of Conservation, Division of Mines and Geology, Office of Strong Motion Studies, Report OSMS 92-09.

Malhotra, P. K., Huang, M. J., Shakal, A. F. (1994) "Seismic Interaction at Separation Joints of an Instrumented Concrete Bridge," *Journal of Earthquake Engineering and Structural Dynamics*, submitted for publication.

Table I. Identification of spike-causing mechanisms in records of Sensors 7, 8 and 10 shown in Figure 4.

| Mechanism | Transverse spikes in records of Sensors 7 & 8 | Shape of longitudinal doublet in record of Sensor 10 | Shape of axial force pulse* | Spike No. |
|---|---|---|---|---|
| 1 | Equal & opposite | | + | 1, 2, 5 & 6 |
| 2 | Equal & opposite | | − | 4 & 7 |
| 3 | Equal & same polarity | | + | 3 |

* + = compressive; − = tensile

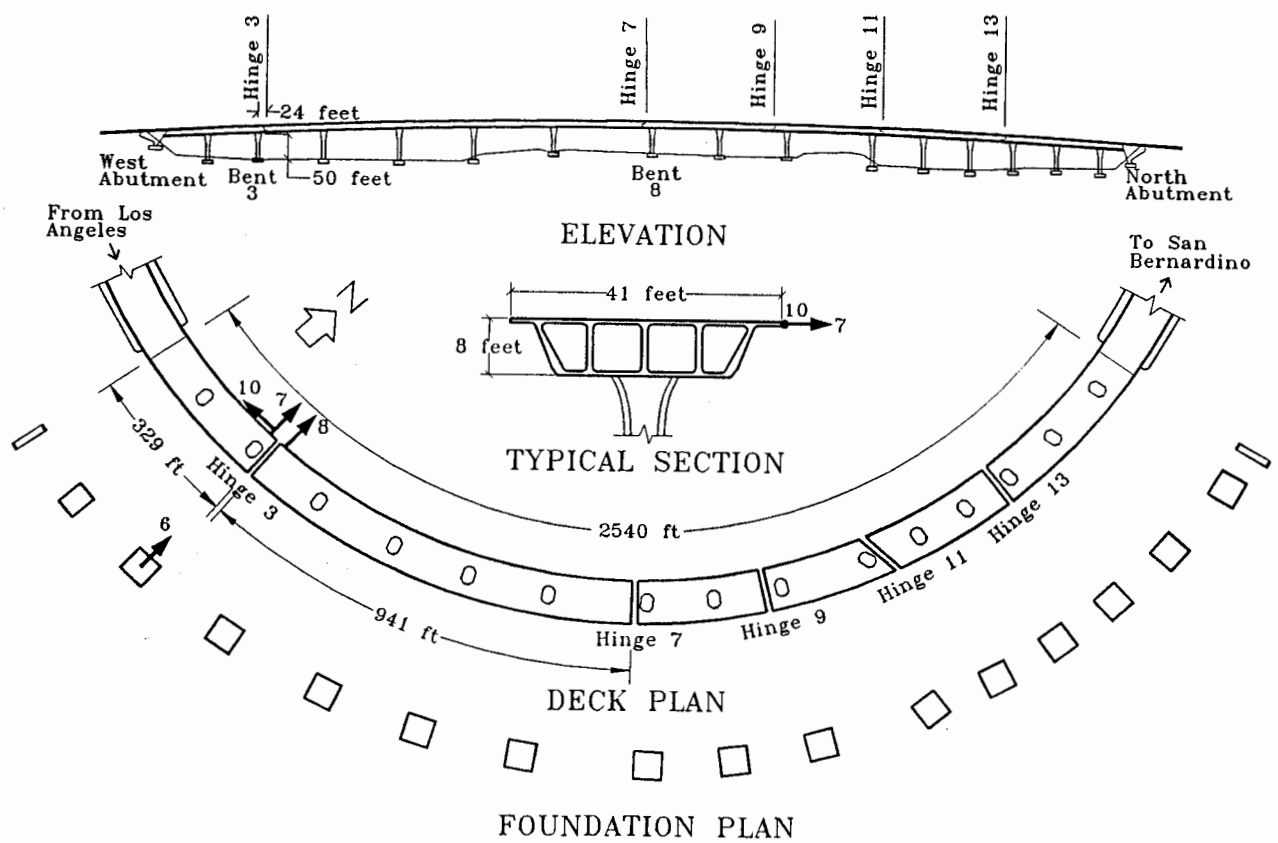


Figure 1. Plan and elevation of the Caltrans I-10/215 interchange bridge in San Bernardino, California showing locations of selected seismic sensors. Only four (6, 7, 8 and 10) of the total thirty-four sensors are shown here. Arrows indicate the positive direction of motion measured by the sensors.

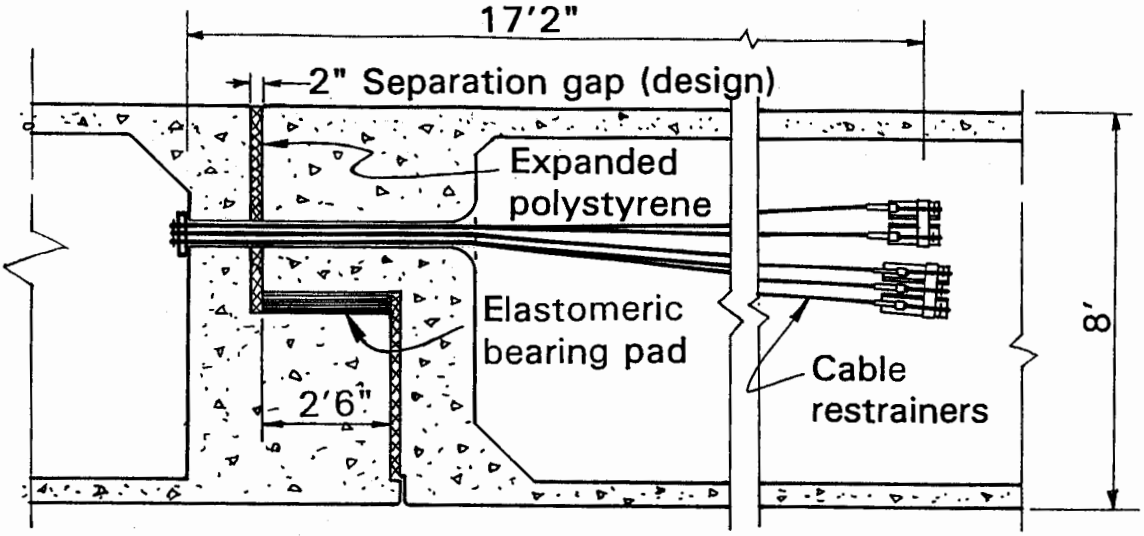


Figure 2. Vertical sections at Hinge 3 showing the separation gap, cable restrainers, and elastomeric bearing pad (from Caltrans construction drawings).

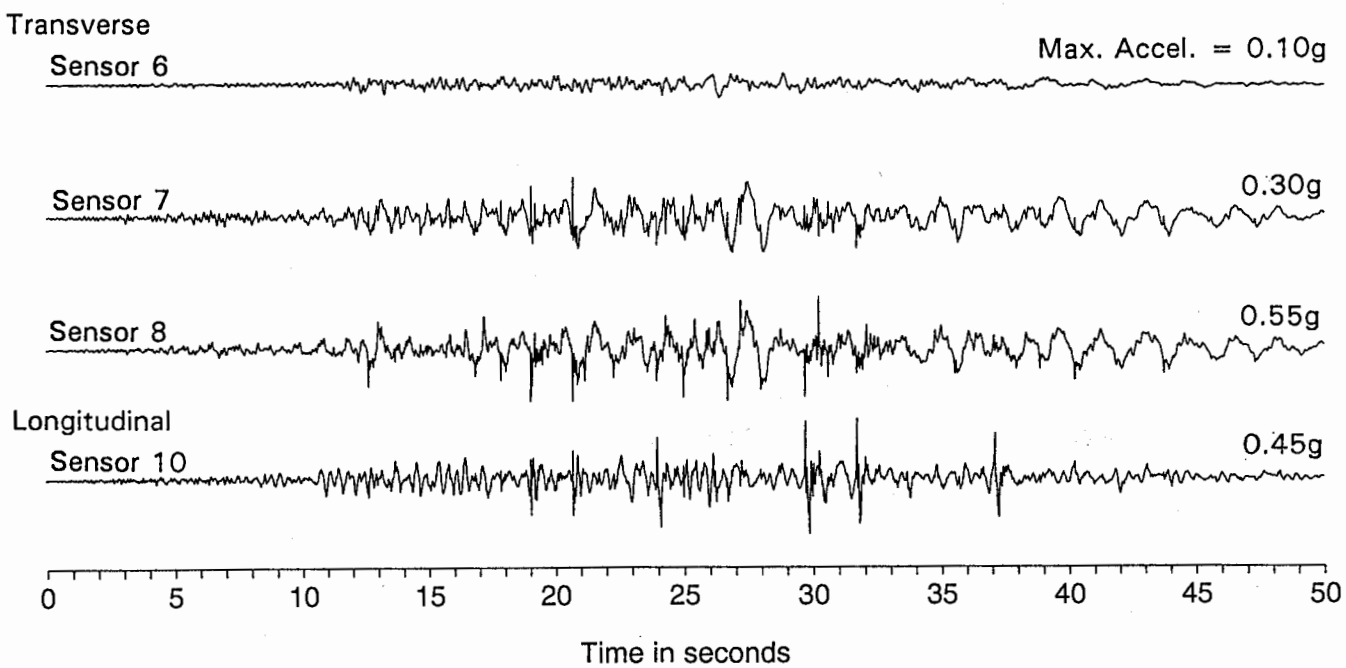


Figure 3. Acceleration records of Sensors 6, 7, 8 and 10 (Figure 1) obtained during the June 28, 1992 Landers earthquake in Southern California.

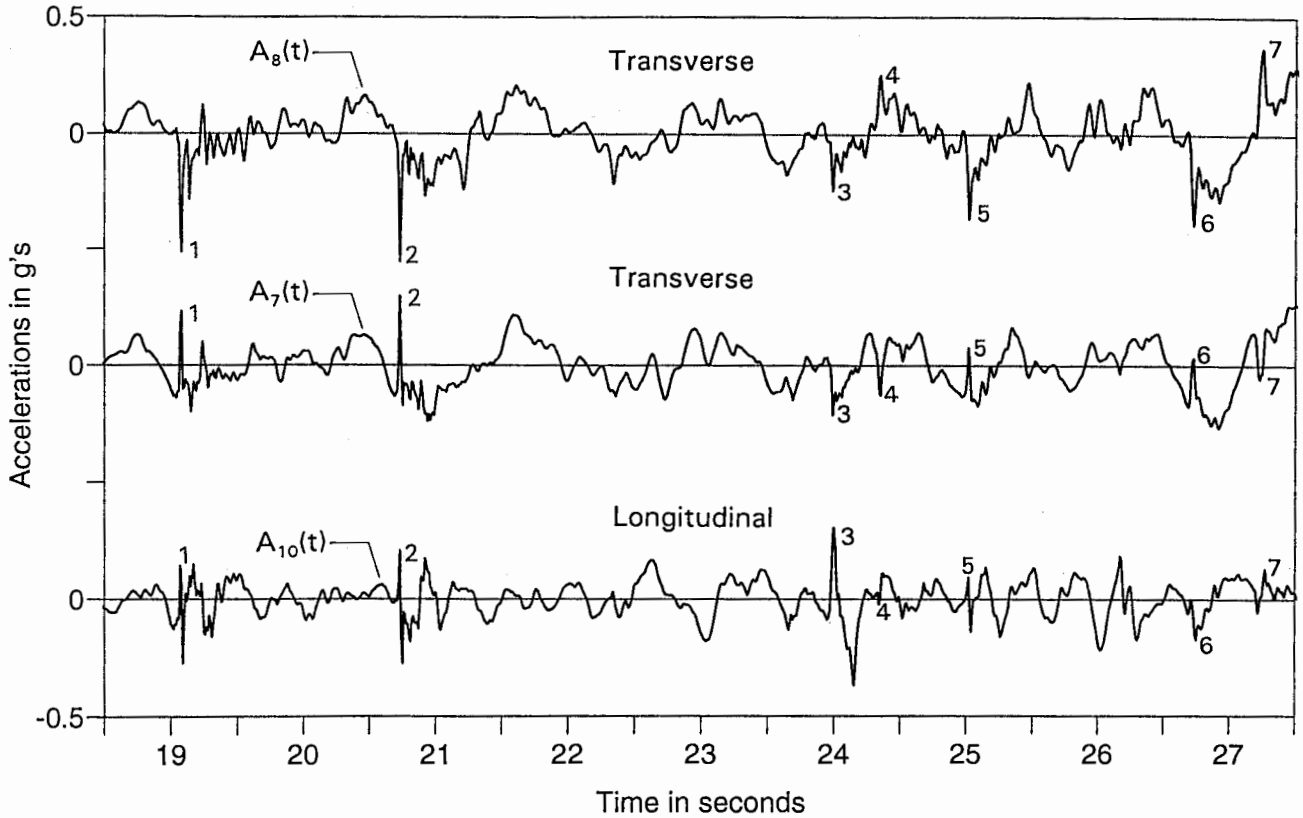


Figure 4. Acceleration records at Hinge 3 from 18.5 to 27.5 seconds into the record, showing simultaneous occurrence of spikes in the transverse, $A_7(t)$ and $A_8(t)$, and longitudinal, $A_{10}(t)$, directions.

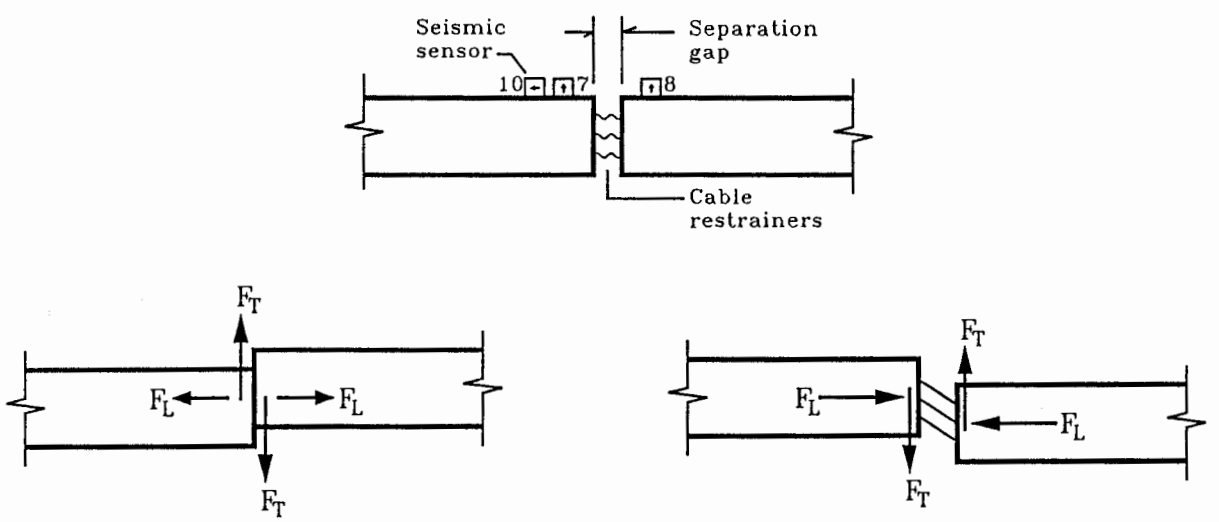


(a) Mechanism 1–Frictional Contact (b) Mechanism 2–Cable Restraint

Figure 5. Plan views at Hinge 3 illustrating interaction Mechanisms 1 and 2. $F_T$=transverse force, $F_L$=longitudinal force; arrows indicate the direction of forces generated.

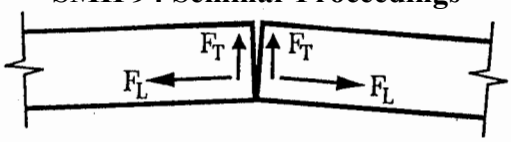


Mechanism 3 Head-on Impact

Figure 6. Plan views at Hinge 3 illustrating interaction Mechanism 3.

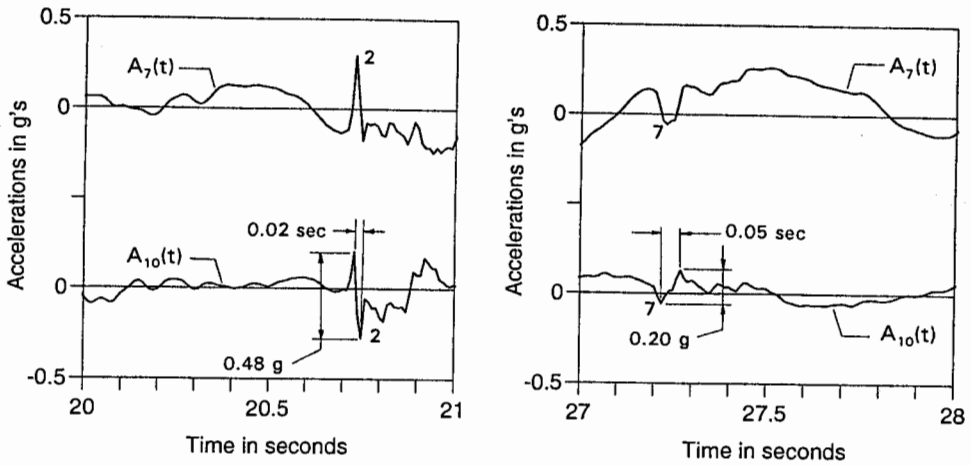


Figure 7. Acceleration records in the vicinity of Spikes 2 and 7 in Figure 4 in the transverse, $A_7(t)$, and longitudinal, $A_{10}(t)$, directions.

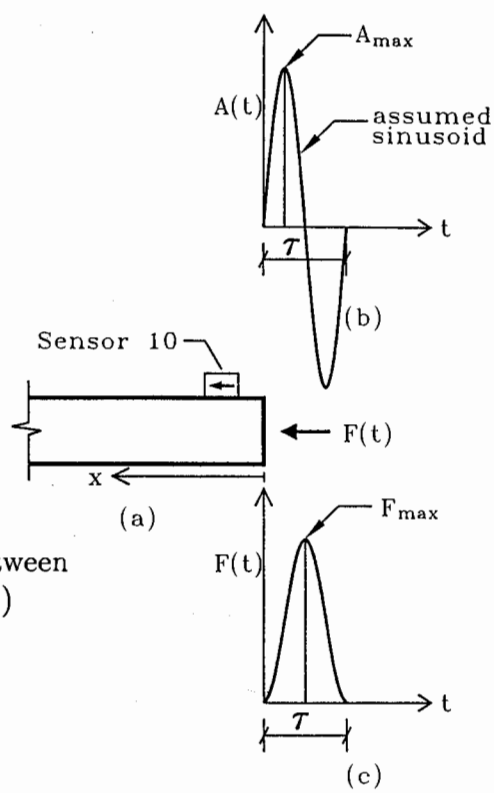


Figure 8. (a) Plan view of the box-girder model used to study the relationship between (b) a hypothetical acceleration spike $A(t)$ similar to those measured by Sensor 10, and (c) the axial force pulse $F(t)$ that would be generated at the end of the box-girder model.